ELSEVIER

Advancing knowledge of electrochemically generated lithium microstructure and performance decay of lithium ion battery by synchrotron X-ray tomography

Fu Sun [1,*,†], Xin He [2,†], Xiaoyu Jiang [3,†], Markus Osenberg [1,4], Jie Li [2,*], Dong Zhou [1,8], Kang Dong [1,4], André Hilger [1,4], Xiaoming Zhu [5], Rui Gao [6], Xiangfeng Liu [6], Kai Huang [7], De Ning [1,4], Henning Markötter [1,4], Li Zhang [1,4], Fabian Wilde [9], Yuliang Cao [3,*], Martin Winter [2,8], Ingo Manke [1]

[1] Helmholtz Centre Berlin for Materials and Energy, Hahn-Meitner-Platz 1, 14109 Berlin, Germany
[2] Helmholtz Institute Münster – Forschungszentrum, Jülich GmbH (IEK 12), Corrensstraße 46, 48149 Münster, D-48149 Münster, Germany
[3] Hubei Key Laboratory of Electrochemical Power Sources, College of Chemistry and Molecular Sciences, Wuhan University, Wuhan 430072, PR China
[4] Institute of Material Science and Technologies, Technical University Berlin, Strasse des 17. Juni 135, 10623 Berlin, Germany
[5] School of Nuclear Technology & Chemistry and Biology, Hubei University of Science and Technology, Xianning 437100, PR China
[6] College of Materials Science and Optoelectronic Technology, University of Chinese Academy of Sciences, Beijing 100049, PR China
[7] Laboratory for Quantum Engineering and Micro-Nano Energy Technology, Faculty of Materials and Optoelectronic Physics, Xiangtan University, Hunan 411105, PR China
[8] MEET Battery Research Center, University of Münster, Corrensstraße 46, 48149 Münster, D-48149 Münster, Germany
[9] Helmholtz-Zentrum Geesthacht, Max-Planck Straße 1, 21502 Geesthacht, Germany

An intrinsic knowledge gap between current understandings obtained experimentally and the underlying working or degradation mechanisms of rechargeable lithium batteries still remains, giving direct rise to application challenges, e.g., safety issues, predicaments in identifying performance-aging factors and dilemmas in guiding further research directions. Against this background, non-destructive and three-dimensional (synchrotron) X-ray tomography that guarantees a direct visual access to inner electrodes has been employed herein to: *in-situ* record the evolution of internal short circuits; characterize the behaviors of widely employed separators; investigate the morphological evolution of Li electrodes under different cycling conditions; and study the degradation mechanisms of Li/carbon cells. By incorporating the currently presented results with the previously published studies on those topics, a complete picture of the degradation mechanism of rechargeable lithium batteries has been painted. This advancement of mechanistic understanding supplies the missing pieces of information to bridge fundamental R&D research activities and practical applications.

Keywords: Lithium ion batteries; Lithium microstructures; Performance degradation/decay mechanisms; in situ/ex situ; SEI

Introduction

Significant breakthroughs in most of electrochemical energy storage systems necessarily require fundamental and comprehensive understanding of their working and degradation mechanisms [1,2]. The lithium ion batteries (LIBs), for example, which were successfully commercialized by SONY in 1991 [3] and afterward revolutionized the powerhouse for personal digital electronic devices [4,5], prevail due to the established knowledge of the solid electrolyte interphase (SEI) layer formed on carbon surface [6,7]. Recent emergence of new electronic devices such

* Corresponding authors.
E-mail addresses: Sun, F. (fu.sun@helmholtz-berlin.de), Li, J. (jie.li@uni-muenster.de), Cao, Y. (ylcao@whu.edu.cn).
† Authors contributed equally to the paper.

https://doi.org/10.1016/j.mattod.2018.11.003

as unmanned aircrafts and robots, along with the immense electric vehicle market, ask for batteries with high energy density than that is available from the state-of-the-art LIB technology [8]. This soaring demand has led worldwide researchers back to the Li metal anode again due to its highest theoretical capacity and lowest electrode potential among all practical anode candidates for rechargeable lithium batteries [9]. However, before becoming a viable battery anode, its long-standing and formidable challenges, i.e., the growth of different shapes of lithium microstructure (LMS, e.g., dendrite [10], whiskers [11], fiber [12], mossy [13], filaments [14], pellet [15], etc., any form that differentiates from solid Li bulk), ineffective SEI layer, and low Coulombic efficiency (CE), have to be overcome. To address these issues, efforts aimed to understand the nature of LMS and SEI by employing electrochemical technique [16], different microscopies [17,18], nuclear magnetic resonance (NMR) [19] or magnetic resonance imaging (MRI) [20], electrochemical quartz crystal microbalance (EQCM) [21], synchrotron X-ray tomography [22], small-angle neutron scattering [23], and compositional analytical technique [24] have been conducted. Recent reports of LMSs by cryo-TEM technique from Zachman et al. [25] and Wang et al. [10] provide further in-depth insights. In parallel, various deliberate strategies designed to alleviate or eliminate the growth of LMS have been proposed, such as lithium metal surface tailoring [26], lithium alloy utilization [27], electrolyte optimization [28], employment of artificial SEIs [29] and passivation/protection layers [30], separator modification [31], and engineered current collectors [32].

These broad investigations have provided a great deal of insight into the working mechanism of lithium metal batteries (LMBs, *v.s.*). However, to the best of authors' knowledge, the correlation between the formidable challenges in LMBs and the aging mechanisms encountered in commercial LIBs, if there is, has not been investigated or established. On the basis of the current understanding of both LMBs and LIBs, several issues draw our further attention. (1) Safety concern. As battery users and manufactures push aggressively for higher energy density, instances of field failures resulting in serious safety threat and socioeconomic risk are increasingly reported [33]. Thus, the detailed mechanism of internal short circuit (ISC), which is directly responsible for battery failure, has to be explicitly revealed. (2) Aging mechanism. The current understanding for the aging of rechargeable lithium batteries is associated with complex interdependencies from intrinsic cell components on one hand (electrode, electrolyte, current collector, separator, etc.) and extrinsic operation conditions on the other hand (temperature, current-rate, voltage range, etc.) [34,35]. In order to realize a good combination of high energy density and extended lifetime of the next-generation batteries, the dominating factor responsible for universal performance decay is important and interesting to be defined [36]. (3) Characterization method. Scrutinizing through the relevant literatures, one can find that electrochemical characterization techniques have been widely used to study the performance of new electrode/electrolyte materials or novel electrode/battery architectures. For example, the CE has been overridingly relied upon to evaluate the cycling efficiency of artificially modified Li electrodes (*v.s.*). Question regarding the single use of characterizing method to evaluate performance improvement arises: to what extent can one single evaluator truly represent the studied electrochemical process, e.g., the CE to the cycling efficiency of Li? [37]. In summary, in order to solve these issues in rechargeable lithium batteries to further enhance their performances, in-depth, sufficient, and comprehensive analytical investigations have to be conducted.

Herein, the non-destructive (synchrotron) X-ray tomography technique, which also guarantees the ability to directly visualize the inner electrode three dimensionally [38], is employed to tentatively fulfill the knowledge gap between research investigations and practical applications. Specifically, the current research consists of four major systematic, comprehensive and inter-related investigations: Section 1 focuses on *in situ* study of the growing Li microstructures, aiming to uncover the elusive evolution behavior of internal short circuits; Section 2 presents investigation results of the phenomenal behaviors/performances of several currently commercialized separators exposed to inconsistently growing lithium microstructure under deep discharge condition, reaching a solid conclusion for future development of separators; Section 3 reports on the unprecedented evolution of Li metal and Li microstructures under different electrochemical cycling conditions, challenging the currently widely accepted assumptions of Li utilization efficiency; Section 4 pinpoints the underlying degradation mechanism of Li/carbon cells by correlating the charge-induced lithium microstructures with that from section 1–3 and also that reported from previous relevant publications, establishing the correlation between the formidable challenges met in LMBs and the aging mechanisms encountered in commercial LIBs. By incorporating the currently presented results with the previously published studies on those concerned issues (for both Li metal and carbon anode), a complete picture of the underlying degradation mechanism of rechargeable lithium batteries has been painted. This advancement of mechanistic understanding opens the possibility to evaluate the reliable degree for previous interpretations that based solely on individual characterizations, as well as to supply the missing pieces of information required to guide future R&D activities.

A total of 30 different electrochemical cells, 3 different beamlines located in 2 synchrotron X-ray facilities (PETRA III-P05 [39] beamline at DESY operated by Helmholtz-Zentrum Geesthacht, Hamburg; beamlines EDDI [40] and BAMline [41] at BESSY II, Berlin) and 1 laboratory X-ray source [42] have been employed in this report. Schematic illustrations of the customized electrochemical cell and the employed beamline set-ups are depicted in Fig. 1. Information of cell state and cycling condition, as well as tomography characterization and data reconstruction procedures, are concisely listed in Table 1, and details of all these information are explicitly specified in Supplementary Materials (SM).

Section 1 in situ monitoring of LMS growth

In this work, an EDDI beamline equipped with fast tomography ability (1.5 min per tomography with resultant resolution of 2.5 μm) was employed to record the growing LMSs occurring in Li symmetrical cells during galvanostatic "discharge". Correlating the morphological evolution of Li metal and LMS and the corresponding electrochemical behavior inside cell No. 1 (as shown in Fig. 2a and e respectively) enables one to directly explore the detailed formation process of ISC. From a series of

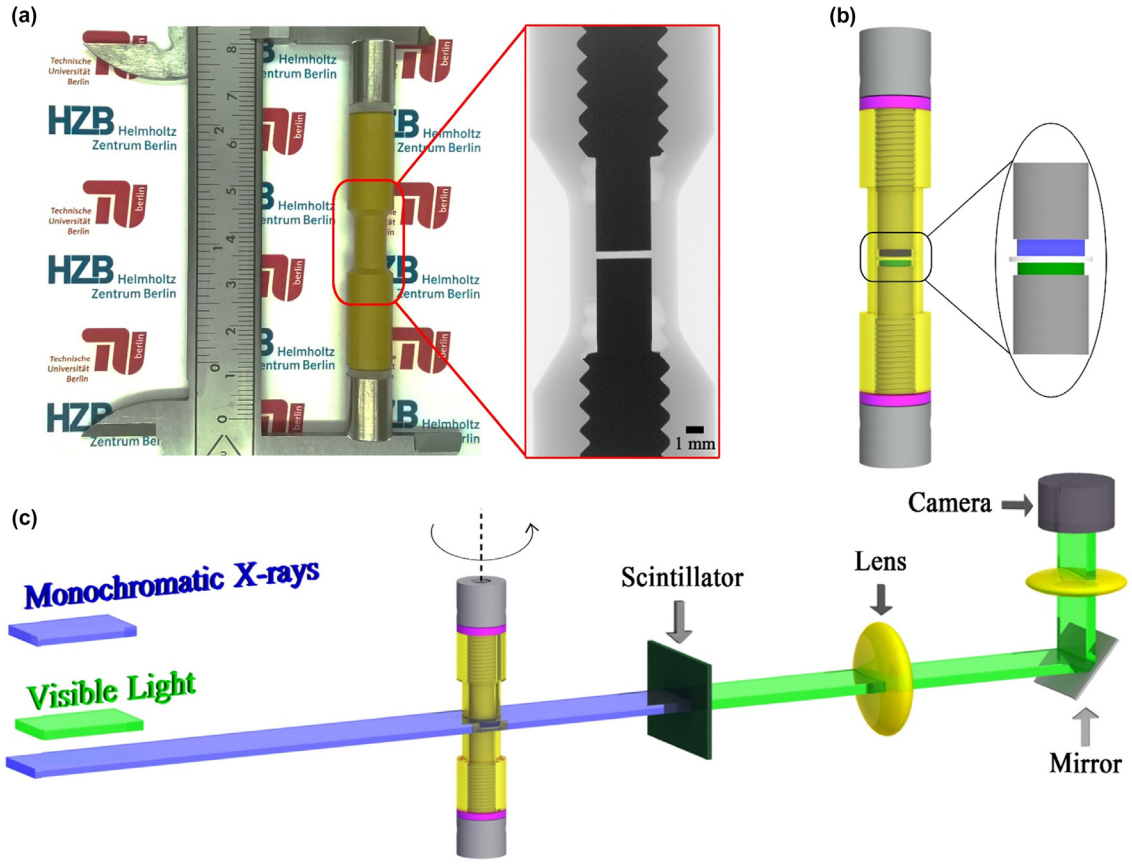

FIGURE 1

Photograph and schematic illustration of the cell and the measurement setup. (a) Photograph of the fabricated cell, the enlarged picture in the red rectangle shows the interior of a blank cell, characterized by the laboratory X-ray setup. (b) Corresponding schematic representation of the cell consisting of a polyamide-imide housing (yellow), two stainless steel screws (light gray), two sealing rings (pink), and a porous separator (white) sandwiched between two electrodes (blue and green). (c) Schematic representation of the experimental setup of the tomography station at the BAMline and EDDI at BESSY II and at the P05 at DESY.

snapshots shown in Fig. 2a, a "bump" structure has gradually evolved on the surface of Li Pos. (positive electrode, note that the positive and negative electrodes are defined during the first discharge process by undergoing lithiation and delithiation processes. This also applies to the rest symmetrical cells), and it pushes the separator upward to the Li Neg. (negative electrode) until the separator cracks (see the last panel with time stamp 08:00, marked by a red square). The preferential accumulation location for the bump structure may stem from an inhomogeneous distribution of electric field [41] or lithium-ion flux [43]. In order to gain more details of the observed electrochemically generated LMS bump, BAMline with a higher resolution (0.438 μm) has been used to characterize cell No. 1 after the EDDI measurement, and the results are shown in Fig. 2b, c (corresponding to the regions marked by red and blue squares in the last panel with time stamp 08:00 in Fig. 2a). It can be discerned that the bump is composed of numerous LMSs, and the separator Celgard 2500 undergoes partial meltdown (pointed by pink arrows). The current findings of ISC using Celgard 2500 share, to some extent, similarities with the previous results that employed Celgard 2325 separator [44]. An overall view of the bump structure is shown in Fig. 2d. (It has to be noted that images of the same cell obtained from different characterization tools generally display different views or perspectives because the starting measurement position is not same, e.g., the enlarged Fig. 2b may not be exactly the same view shown in red rectangle in Fig. 2a (this is also true for laboratory and synchrotron X-ray measurements, see below). It also has to be noted that the 2D images shown in Figs. 2–5 are selected from 2000 to 4000 (based on measurement parameters at different beamlines) images, meaning that some information may not be fully displayed in one selected image.)

Taking the electrochemical behavior into consideration, one can infer that the bump structure is a direct accumulation of electrochemically generated LMSs (EG-LMSs), which are shaped into bump form by reducing the incoming Li^+ fluxes dissolved from Li Neg. and followed or in parallel SEI formation. Note that the dissolution of Li Neg. will concomitantly generate cavities or pits therein. The newly formed EG-LMSs on top of Li Pos. would grow upward and push the polymer separator into these cavities because of the free physical constraints therein. During this process, significant force would be generated and applied to the separator, similar scenario to a puncture/penetration strength test of a separator [45,46]. Eventually, sudden rupture of separator would inevitably occur at the point where the threshold strain value has been exceeded. This process has been vividly demon-

TABLE 1

Investigated cell composition, electrochemical and measurement information. Detailed information is explicitly documented in SM.

	[1]Cell No.	[2]Cell Info. (Neg./Separator/Pos.)	[3]Cycling Info. (D, discharge; C, charge; O, over)	[4]Spatial Resolution (μm)	Figures Info
Sect 1	1	Li/Celgard 2500/Li	D to ISC	2.5	Fig. 2a
				0.438	Fig. 2b–d
	2	Li/Celgard 2325/Li	D to ISC	2.5	Fig. 2h
	3	Li/Al_2O_3-Celgard 2325/Li	D to ISC		Fig. 2i
	p1	Li/Celgard 2500/Li	None	0.438	Fig. S1A, B
	p2	Li/Al_2O_3-Celgard 2325/Li			
Sect 2	4	Li/Celgard 2500/Li	D to ISC	0.438	Fig. 3a2–3
	5	Li/ Celgard 2325 + FS2226 /Li	D to ISC		Fig. 3b2–3
	6	Li/ Celgard 2325 + S240 /Li	D to ISC		Fig. 3c2–3
	7	Li/ Celgard 2325 + GF/D/Li	D to ISC		Fig. 3d2–3
	8	Li/Celgard 2500 + 2325/Li	D to ISC	1.29	Fig. 3e2–3
	9	Li/Celgard 2500 × 2/Li	D		Fig. 3f2–3
	p3-4	Corresponding pristine cell	None	0.876	Fig. S1C–G
	p5-7			1.29	
Sect 3	10	Li/Celgard 2325/Li	250 cycles (cycle/40 min)	1.29	Fig. 4a2–3
	11		94 cycles (cycle/2 h)		Fig. 4b2–3
	12		12.5 cycles (cycle/4 h)	0.438	Fig. 4c2–3
	13		14 cycles (cycle/8 h)		Fig. 4d2–3
	14		4.5 cycles (cycle/20 h)	1.29	Fig. 4e2–3
Sect 4	p8	Li/Celgard 2325/carbon fiber	None	0.876	Fig. S1H
	15		OD		Fig. 5a2–3
	16		OD + C		Fig. 5b2–3
	p9	Li/Celgard 2500/MCMB (meso-carbon micro-bead)	None	0.876	Fig. S1I
	17		OD		Fig. 5c2–3
	18		OD + C	0.438	Fig. 5d2–3
	p10	Li/Celgard 2500/graphite carbon	None	0.876	Fig. S1J
	19		OD		Fig. 5e2–3
	20		OD + C	0.738	Fig. 5f2–3
Abbr.	LMS, lithium microstructure; EG-LMS, electrochemically generated-LMS; Neg., negative; Pos. positive; Cg. Celgard.				

[1] Cell number starts with "p" representing pristine state cell.
[2] See SM for detailed battery assembly procedure.
[3] See the corresponding electrochemical curves and SM for more details.
[4] See SM for detailed measurement parameters.

strated in Fig. 2a. In analogy with the monolayer PP (polyolefin) Celgard 2500 separator, the trilayer Celgard 2325 (PP/PE/PE; PE, polyethylene) separator displays a similar rupture course, as clearly shown in Fig. 2h, apart from an extra layer delamination (see the last panel with time stamp 11:15, pointed by pink arrows). Furthermore, the Al_2O_3-modified Celgard 2325 (Al_2O_3-Celgard 2325) separator, which has been prepared to investigate the effect of ceramic modifying, shows similar behavior as displayed in Fig. 2i. The preparation procedures of the Al_2O_3-Celgard 2325 separator and its parameters are described in the SM. For the deformation and fracture behaviors of the Celgard separators, readers can refer to Ref. [47] and Ref. [48]. (The different time duration before ISC forming among different cells may result from different pressures on the Li electrodes/separators during hand cell-assembly process and/or in-homogeneous current distribution.)

Considering the electrochemical behavior of the studied cells and the morphological evolution of EG-LMSs and separators, one can conclude that the constantly growing EG-LMSs do directly cause deformation and fracture of the separator and give direct rise to ISC, the progress of which mimics a puncture/penetration strength test of a separator [45,46]. The direct visualization of ISC formation process also provides somehow counterintuitive insights into the underlying evolution of ISC, which has been conventionally related to the LMS penetrating the separator. From this section, it is hard to tell whether the bump grows from its root or top during one-directional electrochemical deposition due to the low resolution of EDDI measurement (see more in section 3). However, it can be stated that it is the direct fracture or breakdown of the separator caused straightforwardly by the incessantly growing EG-LMSs that lead to ISCs. Investigations of different separators' properties/behaviors in the presence of growing EG-LMSs and the evolution of EG-LMS and Li anode during different electrochemical cycles are further investigated in Section 2 and Section 3, respectively.

Section 2 behaviors of different separators under growing EG-LMS

To evaluate the behaviors/performances of currently commercialized separators exposing to inconsistently growing EG-LMSs, cells assembled with different separators after deep discharge have been investigated at BAMline or P05. Note that all cells have been measured by the laboratory X-ray instrument (6 μm) at the first place and the reconstructed overall morphological views are shown in the inset figures of their electrochemical curves shown in the first column of Fig. 3. To begin with, another Li symmetrical cell employing Celgard 2500, cell No. 4, has been measured after the ISC occurred (Fig. 3a1), and the

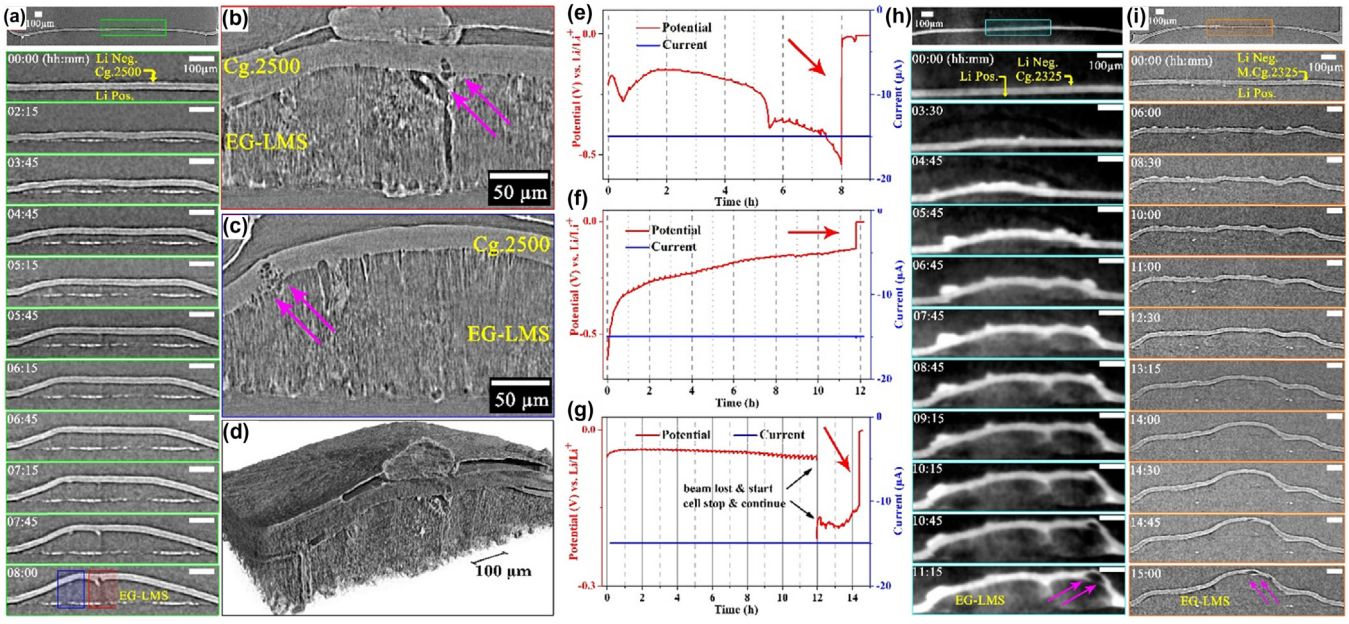

FIGURE 2

In situ monitoring growing lithium microstructures. (a)–(e) show both the inside morphological changes and electrochemical measurements of cell No. 1: (a) the evolution of EG-LMSs during discharge measured at EDDI; (b) and (c) the enlarged part (measured at BAMline) marked in (a) in the last panel with time stamp 08:00; (d) the 3D demonstration and (e) the electrochemical behavior. (f) and (h) show the corresponding results of cell No. 2 assembled with Celgard 2325 separator: (f) the electrochemical curve and (h) the evolution of EG-LMS. (g) and (i) show the corresponding results of cell No. 3 assembled with the Al_2O_3-Celgard 2325 separator in a similar way to that of cell No. 2.

results are shown in Fig. 3a2, a3. The crack or meltdown of the separator can be clearly observed (pink diamonds in a2). In the following, three typically commercialized separators, i.e., glass fiber membrane (Whatman GF/D), nonwoven FS 2226 (Freudenberg), ceramic-coating separator S 240 (Separion PET/ceramic), and the combinational use of Celgard 2325 and 2500, have been representatively studied after deep discharge. (For detailed design motivation and parameters of these separators, readers can refer to Refs. [49,50].) Note that the use of GF/D, FS 2226, and S 240 is jointly accompanied with an additional Celgard 2325. Inside views of un-cycled state from the corresponding cells are shown in SM.

A spectacular morphological change of the inside view of short-circuited No. 5 cell (Fig. 3b1) assembled with FS 2226 + Celgard 2325 separators is shown in Fig. 3b2, b3. It can be seen that the EG-LMSs have grown through the FS 2226 separator and caused an unexpected delamination of Celgard 2325 (pink diamonds in b2). Similar phenomenon can be observed in Fig. 3c2 (pink diamonds), c3, which display the morphological changes of inside view of short-circuited cell No. 6 (Fig. 3c1) assembled with S 240 + Celgard 2325 separators. For the cell No. 7, assembled with GF/D + Celgard 2325, tremendous amount of EG-LMSs have also been discovered, and a different fracture behavior-similar to that of Celgard 2500 (shown in a2) is observed, as shown in Fig. 3d2 (pink diamonds) after its short-circuit (Fig. 3d1). It has to be noted that the EG-LMSs growing through glass fiber membrane have been previously reported [51]. Summarizing these direct observations, one can conclude that these three separators (GF/D, FS 2226, and S 240), although have the advantage of high thermal stability, low thermal shrinkage, and high electrolyte uptake ability, are not suitable for high-energy rechargeable lithium batteries because their relatively large pores cannot prevent/restrain the EG-LMS growing through. In order to investigate the role of the mechanical stability of separators in the presence of the growing EG-LMSs, cell No. 8 assembled with Celgard 2325 + Celgard 2500 and cell No. 9 assembled with two Celgard 2500 have been investigated, and the results are shown in Fig. 3e2, e3 and Fig. 3f2, f3, respectively. Both cells endure longer discharge time (Fig. 3e1, f1) compared to that of cells assembled with one polymer separator (a1–d1). Specifically, the inside views of Fig. 3e2 (showing EG-LMSs puncturing through 2 separators after ISC) and Fig. 3f2 (showing no EG-LMSs puncturing through) demonstrate that increasing the puncture strength and mechanical stability may, to some extent, prolong the usage time before final cell failure (in f1 the cut-off voltage of −3 V is automatically set by the cycler).

Given these above comparative investigations, it is therefore convincing to draw a conclusion that improving the puncture strength and overall mechanical strength property is quite important for the development of separators. Separators possessing relatively larger pores and weaker mechanical strength are not suitable for high energy rechargeable lithium batteries where significant amounts of EG-LMSs may be generated (see also section 4). Separators modified with ceramic particles may also not possess sufficient mechanical strength to protect their integrity or to prevent/restrain the EG-LMSs growing-through (see also section 1). Applying the knowledge learned herein to the cell for SAMSUNG Galaxy Note 7, which employs a polymer of 4.5-μm-thick monolayer coated with 1-μm-thick Al_2O_3 ceramic particles as separator, may explain why it unavoidably fails under

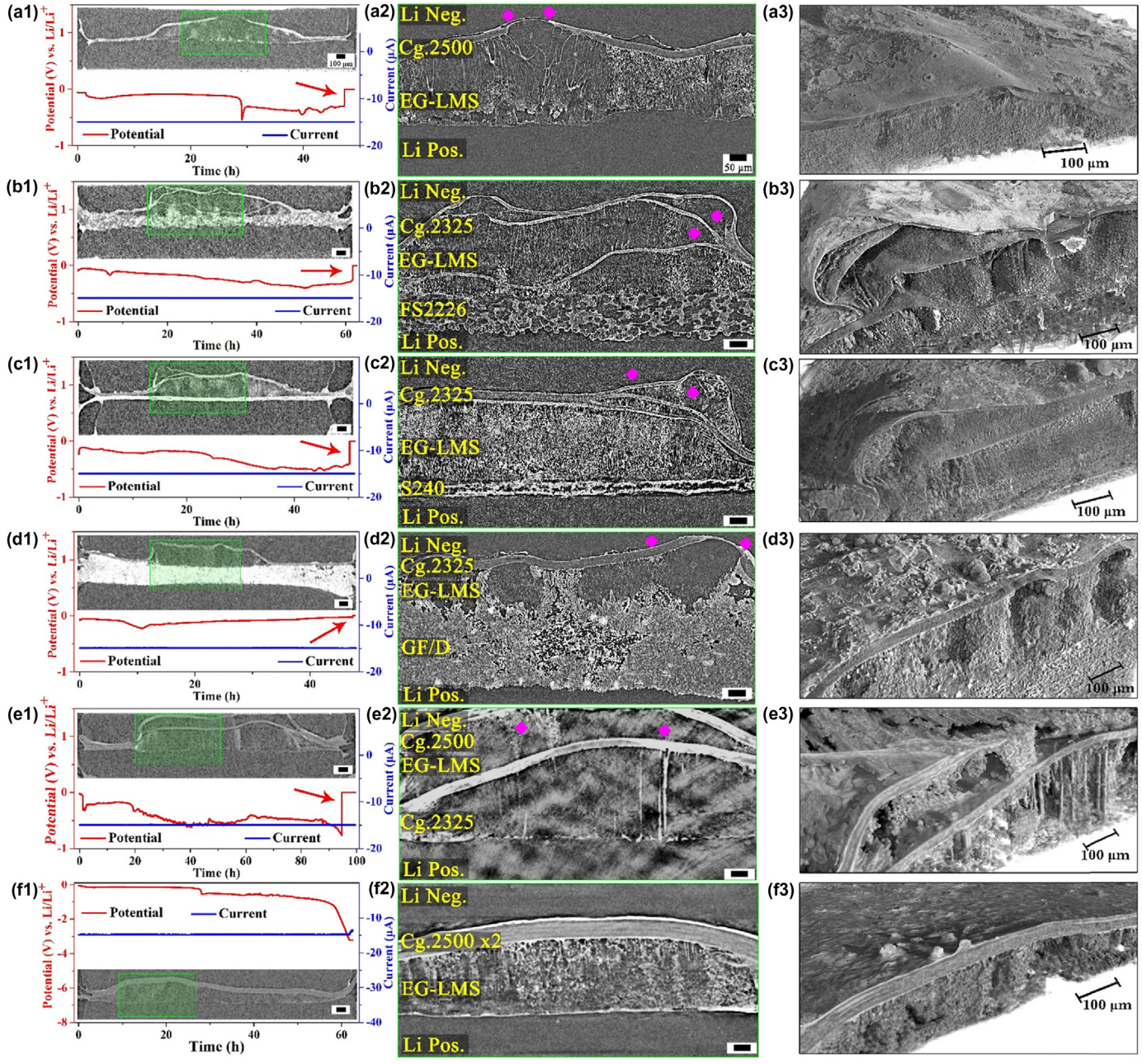

FIGURE 3

Investigations of the impact of different separators on the growth behavior of EG-LMSs. (a1)–(a3) show the results from an internal short circuited cell No.4 assembled with a single Celgard 2500 separator. (b1)–(b3) show the results from cell No.5 assembled with FS 2226 + Celgard 2325 separators. (c1)–(c3) show the results from cell No. 6 assembled with S 240 + Celgard 2325 separators. (d1)–(d3) show the results from cell No. 7 assembled with GF/D + Celgard 2325 separators. (e1)–(e3) show the results from cell No. 8 assembled with Celgard 2325 + Celgard 2500 separators. (f1)–(f3) show the results from cell No. 9 assembled with two Celgard 2500 separators. The first column shows the cell's electrochemical curves within each shows the resliced reconstructions measured by the laboratory X-ray instrument. The second column shows the selected 2D slices measured from BAMline (cell No. 4–7) and P05 (cell No. 8–9). The third column shows correspondingly the 3D demonstration.

particular conditions [52] (see more detailed investigation elsewhere [53]).

Section 3 evolution of Li and EG-LMS under different cycling conditions

An important point that to what degree the electrochemical measurement (the obtained CE) can truly represent the Coulombic efficiency (CE) during cycling of Li has not been well discussed. However, it is important to consider it because the CE is widely adopted in battery community. Herein, in order to answer this question, cells No. 10–14 experiencing different amount of Coulomb (C) or capacities of transported charges during dis/charge-mimicking various electrochemical tests adopted by different researchers to investigate Li cycling efficiency have been measured, and their internal morphological changes are shown in Fig. 4.

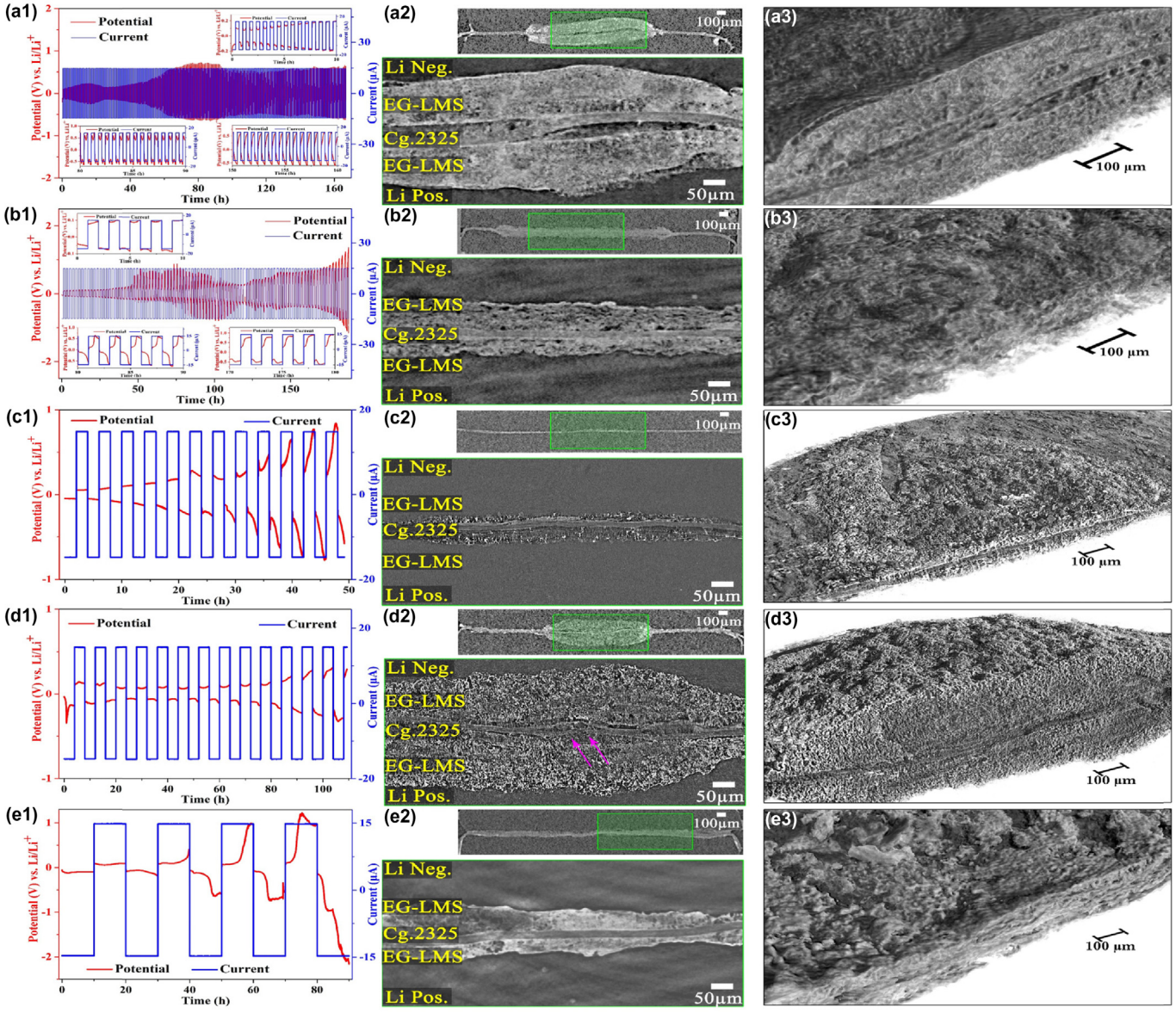

FIGURE 4

Correlating the interior morphological evolution of Li electrodes and EG-LMSs to the overall cell's electrochemical behavior. (a1)–(a3) show the results of cell No. 10 cycled for 250 cycles. (b1)–(b3) show the results of cell No. 11 cycled for 94 cycles. (c1)–(c3) show the results of cell No. 12 cycled for 12.5 cycles. (d1)–(d3) show the results of cell No. 13 cycled for 14 cycles. In (d2), the pink arrows point to the breakdown of the separator. (e1)–(e3) show the results of cell No. 14 cycled for 4.5 cycles. The first column shows the electrochemical curves. The second column shows the selected 2D slices reconstructed from laboratory X-ray instrument measurement (top panel) and BAMline (cell No. 12–13) or P05 (cell No. 10–11 and 14) measurement (bottom panel). The third column shows correspondingly the 3D demonstration.

Taking an overall look at Fig. 4, one can find that newly formed EG-LMSs, which distinguish themselves easily from original solid Li bulk, accumulate on top of Li electrodes independent of the transported charge amount. Moreover, comparing Fig. 4a2–e2, one can draw a conclusion that the total amount of formed EG-LMSs is roughly proportional to the total amount of C transferred during cycling (corresponding cycling curves a1–e1). Taking the underlying evolution mechanisms of plated/stripped LMSs into consideration [54], one can reasonably conjecture that these EG-LMSs generated on top of original Li electrode result from a synergistic effect of electrochemical stripping of original bulk Li during dissolution (generating various of cavities), and afterward electrochemically/chemically generated EG-LMSs during subsequent deposition (occupying subsequently the generated cavities, see details in section 1 and elsewhere [54]). The root cause for the observed morphological evolution of Li electrodes and EG-LMSs is that most of the EG-LMSs are electrochemically inactive, and it is the original Li bulk instead of the nascent EG-LMSs that undergoes electrochemical stripping. Moreover, from this picture, one can rationally infer that the newly generated EG-LMSs have to be deposited/plated directly on top of original Li bulk, pushing the previously formed ones upward. This conclusion can be reached when considering that most of the EG-LMSs are electrochemically inactive

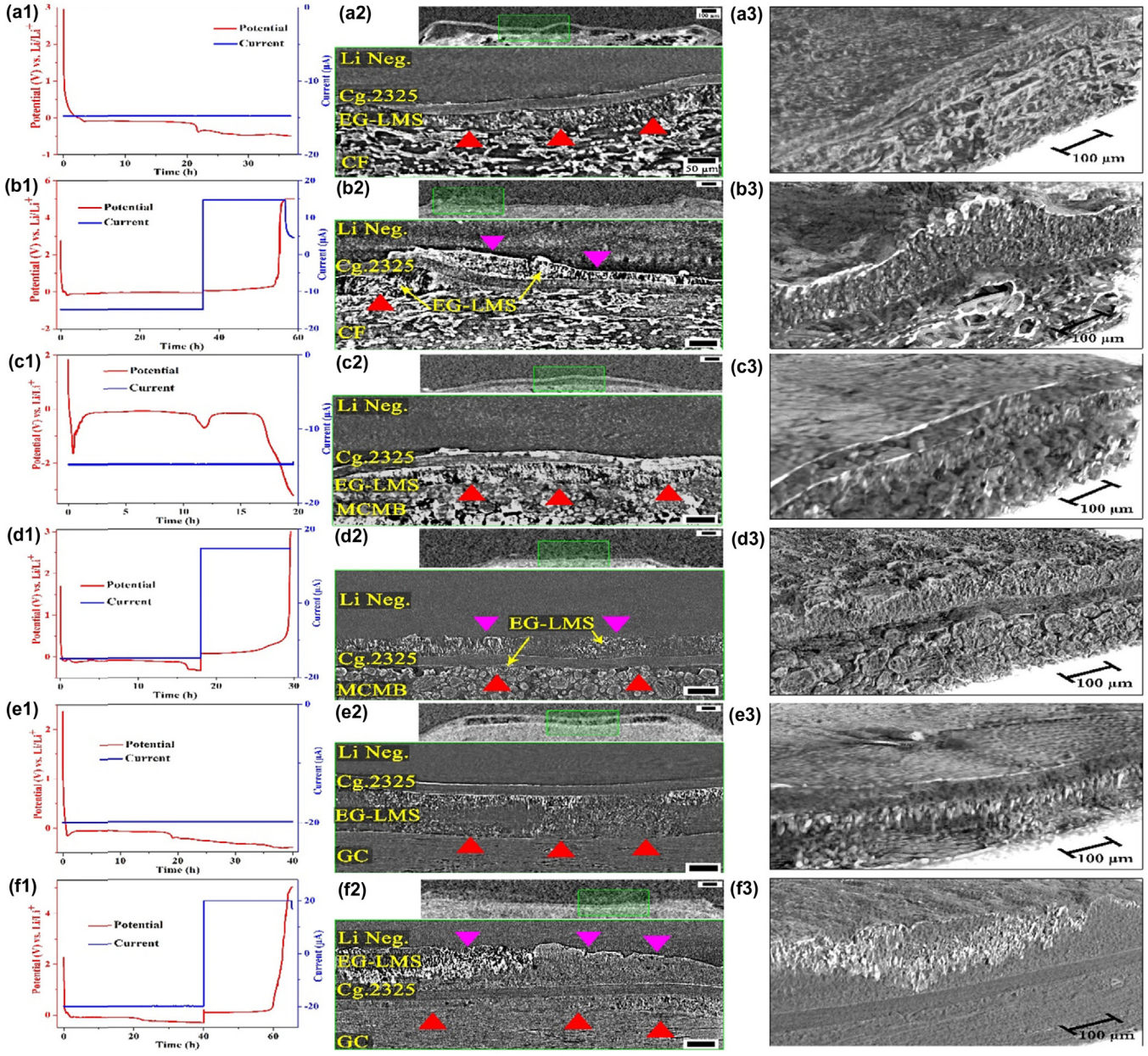

FIGURE 5

Correlating the interior morphological evolution of EG-LMSs to the overall cell's performance decay. (a1)–(a3) show the results of cell No. 15. (b1)–(b3) show the results of cell No. 16. (c1)–(c3) show the results of cell No. 17. (d1)–(d3) show the results of cell No. 18. (e1)–(e3) show the results of cell No. 19. (f1)–(f3) show the results of cell No. 20. The first column shows the electrochemical curves. The second column shows the selected 2D slices reconstructed from laboratory X-ray instrument measurement (top panel) and BAMline measurement (bottom panel). The third column shows correspondingly the 3D demonstration.

(electronically isolating) and the incoming Li^+ can only be reduced at the locations where electrons are directly available (the bulk Li). Indeed, this growth behavior of EG-LMSs during cycles has been experimentally validated [55].

The evolved Li electrodes and EG-LMSs in Li symmetrical cells after electrochemical cycling challenge the foundation of evaluating their cycling efficiency by CE, which assumes that it is the EG-LMSs that undergo stripping. It also raises another interesting question: to what certain extent the EG-LMSs are electrochemically reversible (see the final discussion at the end of this report)? Furthermore, it casts doubt on the reliability of the information obtained by employing Li metal as counter electrodes to evaluate electrochemical properties of new electrode materials and/or architectures because of the electrochemically inactive EG-LMSs [56]. The final question that has to be asked is the correlation between these EG-LMSs observed in LMBs and the aging mechanisms encountered in commercial LIBs under cycling condition (see section 4).

Section 4 correlation between EG-LMSs and performance decay of LIBs under cycling condition

Significant efforts have been taken to clarify the underlying aging mechanisms of LIBs under different cycling conditions

and it has been generally acknowledged that the irreversible loss of active Li inventory in form of a thick layer on top of carbon electrode is the major cause [57,58]. This thick layer, which has been given different names, e.g., untypical layer [59], anode surface [60], lithium compound deposition [61], μm-thick covering layer [62], resistive interface layer [63], additional deposit layer on top of the SEI [64], or SEI [65] by different research groups, has been confirmed to be composed mostly of Li by inductively coupled plasma optical emission spectroscopy (ICP-OES) [66], glow discharge optical emission spectroscopy (GD-OES) [60], and further osmium tetroxide (OsO_4) staining [67]. It is also important to mention that another classification for this thick layer is Li deposition [68] or Li plating [69,70,71]. Note that similar thick layers have also been discovered on top of cycled Li electrodes in LMBs and have been named by e.g., crust layer [72], degradation layer [73], lithium porous interface [74], and secondary SEI [75]. However, it is still not clear how the observed thick layer that traps significant amount of Li affects the irreversible capacity loss in rechargeable lithium batteries (both LIBs and LMBs). The knowledge gap between our understandings and the experimental observations has been tentatively fulfilled in terms of the electrochemically inactive EG-LMSs, as shown below.

Over-lithiation of carbon electrode (i.e., over discharge of Li/C half-cell or overcharge of carbon based LIBs) has been adopted instead of long-term cycling due to the limited allocated beamtime (For long-term cycling investigations, readers can refer to previous reports [59–64]). Three types of carbon are investigated here: the carbon fiber (CF), the mesocarbon microbead (MCMB), and graphite (G) foil. It can be observed from Fig. 5a2 that a great deal of EG-LMSs are generated on top of the CF electrode (red triangles) after over-discharge (Fig. 5a1). This is in good agreement with previously reported phenomenon of over-lithiated carbon electrode in LIBs [76–78]. Unexpectedly, after charge of the over-discharged cell No. 16 (i.e., delithiation of the over-lithiated carbon, Fig. 5b1), significant amount of EG-LMSs are still present on top of carbon electrode (red triangles in b2) even though the charging potential has been raised to 5 V (Fig. 5b1), together with the newly formed EG-LMSs on top of Li electrode (pink triangles in b2). Correlating the capacity difference obtained electrochemically during charge and discharge (b1) with the remnant EG-LMSs (red triangles, b2), one can conclude that it is these electrochemically inactive EG-LMSs trapping a significant amount of Li (locate on top of carbon electrode) that cause direct capacity decay during charging. Similar scenarios are shown in other carbon forms (MCMB, c2–d2; G, e2–f2). Recalling the conclusion that the surface chemistry of any anodes polarized to low potential (close to Li deposition, i.e., 0 V *vs* Li/Li^+) is similar to that of Li surface in spite of their different properties drawn by Aurbach et al. [79,80], it can be concluded that the EG-LMSs observed on top of Li electrodes in section 1–3 possess the same nature as that observed on top of carbon electrodes and Li electrodes in section 4. As a matter of fact, the potential of carbon electrode *vs* Li/Li^+ has been frequently reported to decrease below 0 V *vs* Li/Li^+ by employing a three-electrode design during charging of LIBs [81–85], similar to all conditions where EG-LMSs are generated on top of Li or carbon electrodes reported here (all four sections herein and previous relevant reports). Moreover, recent confirmation of EG-LMSs grown on graphite anode studied by electron paramagnetic resonance spectroscopy [85] and on Li anode investigated by NMR [86] provides further experimental evidence for the conclusion.

The current demonstration of EG-LMSs on top of carbon electrodes is significant and meaningful. It implies that the EG-LMSs generated in Li symmetrical cells are actually the same as those formed on top of Li electrodes in LMBs. Moreover, it clearly explains the capacity degradation phenomena in terms of the electrochemically inactive EG-LMSs, which has been widely reported but insufficiently discussed [56]. Finally it provides a global picture of the degradation mechanisms of rechargeable lithium batteries (both LMBs and LIBs) by unifying all previously reported relevant research results together, and as a result, practical research directions for future R&D of current- and next-generation rechargeable lithium batteries can be drawn. The schematic illustration of the current findings is succinctly shown in Fig. 6.

The current paper sheds new insights into the elusive evolution mechanisms of ISC, provides judicious guidelines for future development of separators, challenges the widely used

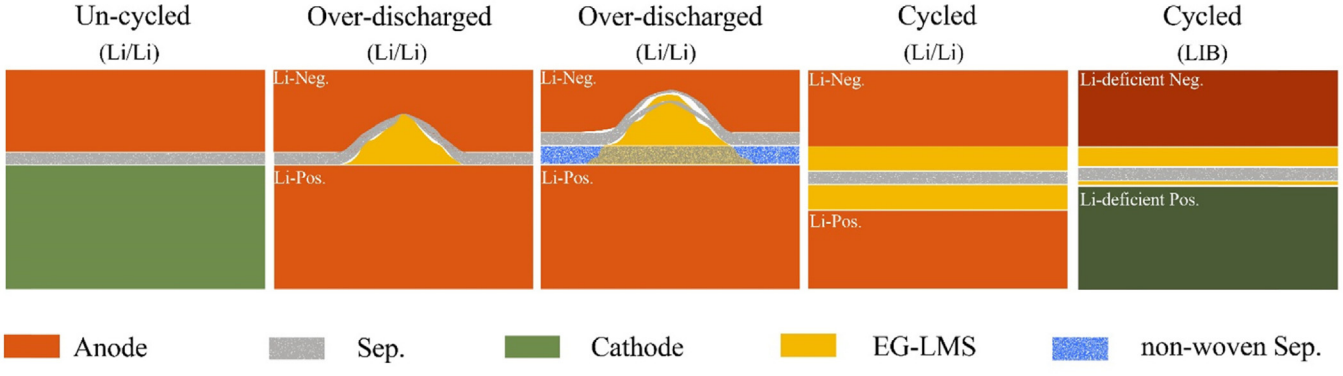

FIGURE 6

Schematic illustration of the interior morphological changes of EG-LMSs in LIBs and LMBs under different cycling conditions. From left to right: the un-cycled cell; the over-discharged Li symmetrical cell assembled with one polymer separator; the over-discharged Li symmetrical cell assembled with one polymer separator and one non-woven separator; the cycled Li symmetrical cell and the cycled LIBs. (For detailed morphological evolution of EG-LMSs during different cycles, readers can refer to Refs. [54,74]; for SEI generated on top of cathodes, readers can refer to Refs. [87,88].)

evaluation method of CE for characterizing Li cycling efficiency, and pinpoints the dictating factor responsible for universal performance decay of rechargeable lithium batteries. In addition, it enables us to reveal or reinterpret previously reported phenomena by combining the currently learned lessons, advancing and deepening our current knowledge.

(1) Enhanced understanding of SEI, lithium plating, and aging mechanism

The theory of SEI was established in 1979 by Peled to explain the electrochemical behavior of alkali and alkaline earth metals in non-aqueous battery systems [6], and later on, Aurbach had contributed significantly to its development by rigorously studying the correlation of the nature of electrolyte with the compositions of SEI on different anodes [89]. (For detailed reviews on the SEI, readers can refer to Ref [7,87–90].) With a closer inspection of the development of SEI theory, one can notice that most of the previous reports concentrated solely on the surface morphologies or compositions of un-cycled or short-term cycled anodes, paying insufficient attention to their cross-sections. Recently reported thick layers (10–100 μm *vs* 10–100 Å of originally supposed SEI thickness), characterized from the cross-sections of long-term cycled negative electrodes, frequently cast questions on the formation process of SEIs and challenges our understanding of their evolution mechanism. Later on, Aurbach had tried to explain the gradual thickening of the surface layer upon prolonged cycling by a dynamic mechanism of SEI breakdown and repair [91], and the latest investigations by employing nanoscale imaging has been devoted to elucidating the growth/dissolution of LMS [11] and its SEI [18] to further contribute to our understanding. However, basic questions still remain. For example, to what degree the EG-LMSs can be electrochemically reversible? It has been reported by some researchers that two thirds of the thick layer can be removed following discharge [60]; others claim only 23% [68].

On the other hand, the insufficient understanding of the correlation among SEI, EG-LMSs, and battery performance decay has led to some improper interpretations. For example, suggestions, such as the de-activated carbon negative electrode [92] or the de-lithiated (Li-deficient) cathode [93], are mainly responsible for battery aging have been proposed. Researchers have found in their studies the presence of the thick EG-LMSs, yet they did not correlate them to the observed performance decay [63]. Others conclude that the new EG-LMSs deposit mainly on the outer layer of previously formed EG-LMS layer [68]. On the basis of current investigations, it seems reasonable to suggest that replenishing sufficient Li (ions) to supply/compromise the depleted active Li (ions) may extend the cycle life of LIBs if the EG-LMSs are mostly electrochemically inactive. Actually, it has been reported that the failed LIBs, after adding adequate amount of electrolyte, can be directly recovered [94]. Furthermore, one may also rationally argue that the performance of the failed carbon negative electrode may be re-activated by disposing of its EG-LMS layer. This theoretical hypothesis has been experimentally confirmed via washing the aged carbon electrodes to regain the lost performance [95]. These reports contribute to understanding the underlying correlations among SEI, EG-LMSs, and performance degradation mechanisms of LIBs.

(2) Judicious selection of diagnostic methods

To establish a clear and thorough understanding of the working and decaying mechanisms of a battery, it is necessary to use comprehensive and complementary analytical strategies to obtain an in-depth view. Reviewing relevant literatures, one can find that the electrochemical characterizations have been widely used because of their easy access and non-destructive advantages. However, to gain a more comprehensive and complementary information, morphological changes of active electrode materials, which did not receive sufficient attentions in most publications, are actually a direct result of the electrochemical or physicochemical phenomena that straightforwardly dictate the performance of a battery. Several reports including morphological inspections have been published, yet the presented pictures have very low spatial resolutions and limited representability, and thus sufficient and reliable conclusions could not be drawn [96]. From the current observations (morphological results of low and high resolution cannot be detected or revealed by electrochemical characterizations), it is suggested that sufficient morphological characterizations have to be linked together to other diagnostic tools to reach more reliable conclusions.

(3) Modeling for ISC or battery aging

Proposed modeling either for elucidating ISC or battery aging can simulate/fit the apparently observed phenomena. However, the ability of predicting service life before ISC and/or estimating capacity retention of a working LIB under specific operation modes, is missing. This lack of reliable predictability can be largely attributed to without taking the electrochemically inactive EG-LMSs into consideration. It is suggested that future simulation modeling capturing the true dynamic decaying mechanism should be developed for the implementation of a reliable and trustworthy battery management system [33].

(4) Future research directions

On the basis of these in-depth discussions, it is suggested that more and more future research attentions should be given to the nature of SEI, EG-LMSs, and their correlation to the overall cell degradation mechanisms. Moreover, developing novel electrolyte that is electrochemically or kinetically stable with anode materials should be equally important. Actually, Gerald H. Newman [97], who was responsible for investigating the first rechargeable Li metal-based batteries in Exxon Research & Engineering Co. during 1980s, concluded that determining a proper electrolyte in which a Li metal can be repeatedly cycled was a prerequisite for its successful commercialization [97]. A new form of liquefied gas electrolyte has been reported recently [98]. However, electrolyte of safer and more environmental friendless is more desirable. For the recently emerging solid-state electrolyte, it is suggested that more investigations are required before reaching a solid conclusion for its role in preventing EG-LMSs growth [99]. Last but not least, the obtained knowledge and research

diagnostic ideas of EG-LMSs presented here should be applied to other rechargeable battery system based on sodium-ion [100], magnesium-ion [101], potassium-ion [102], calcium-ion [103], fluoride-ion [104], dual-ion [105,106,107], or even aqueous rechargeable battery technology [108] because similar microstructures resembling currently observed EG-LMSs after long-term cycling have already been found.

Acknowledgments

We thank Dr. Heinrich Riesemeier, Dr. Paul H. Kamm and Dr. Fabian Wilde for their valuable assistance at beamlines. We thank engineer Norbert Beck and John Schneider for fabricating the beamline battery. This work is sponsored by China Scholarship Council, National Key R&D Program of China (No. 2016YFB0100200) and is partially funded by the German Research Foundation, DFG (Project No. MA 5039/4-1).

Fu Sun, Henning Markötter, Kang Dong, and Ingo Manke designed the cell. Fu Sun, André Hilger, Kang Dong, Markus Osenberg, Dong Zhou, De Ning, Li Zhang, and Henning Markötter conducted the characterizations at synchrotron facilities. Xin He, Jie Li, and Martin Winter contributed mainly to the experiments of section 2-3. Xiaoyu Jiang, Xiaoming Zhu, and Yuliang Cao contributed mainly to the experiments of section 1–2. Rui Gao, Kai Huang, and Xiangfeng Liu contributed mainly to the experiments of section 3–4. All authors contributed to the data interpretation and the discussion of the presented results.

The authors declare no competing financial interest.

Appendix A. Supplementary data

Supplementary data to this article can be found online at https://doi.org/10.1016/j.mattod.2018.11.003.

References

[1] Y. Cohen, D. Aurbach, Rev. Sci. Instrum. 70 (1999) 4668.
[2] G. Tan et al., Nat. Energy 2 (2017) 17090.
[3] A. Yoshino, Angew. Chem. Int. Ed. 51 (2012) 5798.
[4] F. Sun et al., J. Power Sources 321 (2016) 174.
[5] X. He et al., Nano Energy 27 (2016) 602.
[6] E. Peled, J. Electrochem. Soc. 126 (1979) 2047.
[7] E. Peled, S. Menkin, J. Electrochem. Soc. 164 (2017) A1703.
[8] R. Schmuch et al., Nat. Energy 3 (2018) 267.
[9] D. Lin et al., Nat. Nanotechnol. 12 (2017) 194.
[10] X. Wang et al., Nano Lett. 17 (2017) 7606.
[11] A. Kushima et al., Nano Energy 32 (2017) 271.
[12] Brian E. Conway, John O'M. Bockris, Modern Aspects of Electrochemistry, Springer, Boston, MA, 1972.
[13] P. Bai et al., Energy Environ. Sci. 9 (2016) 3221.
[14] K.N. Wood et al., ACS Energy Lett. 2 (2017) 664.
[15] X. Xu et al., J. Energy Storage 13 (2017) 387.
[16] G. Bieker et al., Phys. Chem. Chem. Phys. 17 (2015) 8670.
[17] G. Rong et al., Adv. Mater. 29 (2017) 1606187.
[18] Y. Li et al., Science 358 (2017) 506.
[19] R. Bhattacharyya et al., Nat. Mater. 9 (2010) 504.
[20] H.J. Chang et al., J. Am. Chem. Soc. 137 (2015) 15209.
[21] C.A. Berger et al., ChemElectroChem 4 (2017) 261.
[22] D.S. Eastwood et al., Chem. Commun. 51 (2015) 266.
[23] H. Xin et al., Adv. Mater. Interfaces 4 (2017) 1601047.
[24] D. Aurbach et al., J. Electrochem. Soc. 134 (1987) 1611.
[25] M.J. Zachman et al., Nature 560 (2018) 345.
[26] B. Jens et al., Adv. Mater. Interfaces 4 (2017) 1700166.
[27] X. Liang et al., Nat. Energy. 2 (2017) 17119.
[28] H. Yu et al., ACS Energy Lett. 2 (2017) 1296.
[29] X.-B. Cheng et al., Chem 2 (2017) 258.
[30] K. Liu et al., Adv. Mater. 29 (2017) 1603987.
[31] Y. Liu et al., Nat. Energy. 2 (2017) 17083.
[32] S. Matsuda et al., ACS Energy Lett. 2 (2017) 924.
[33] X. Feng et al., Energy Storage Mater. 10 (2018) 246.
[34] P. Keil, A. Jossen, J. Energy Storage 6 (2016) 125.
[35] A. Friesen et al., J. Power Sources 334 (2016) 1.
[36] M. Yilmaz, P.T. Krein, IEEE T. Power Electr. 28 (2013) 2151.
[37] D. Lu et al., Adv. Energy Mater. 5 (2015) 1400993.
[38] M. Ebner et al., Science 342 (2013) 716.
[39] F. Wilde et al., AIP Conf. Proc. 1741 (2016) 030035.
[40] J. Márquez et al., Chem. Mater. 29 (2017) 9399.
[41] F. Sun et al., ACS Appl. Mater. Interfaces 8 (2016) 7156.
[42] F. Sun et al., Appl. Surf. Sci. 399 (2017) 359.
[43] L. Zielke et al., ChemElectroChem 3 (2016) 1170.
[44] F. Sun et al., ACS Energy Lett. 2 (2017) 94.
[45] S. Kalnaus et al., J. Power Sources 378 (2018) 139.
[46] X. Zhang et al., J. Power Sources 327 (2016) 693.
[47] P. Arora, Z. Zhang, Chem. Rev. 104 (2004) 4419.
[48] J. Chen et al., RSC Adv. 4 (2014) 14904.
[49] M. Kirchhöfer et al., Int. J. Mol. Sci. 15 (2014) 14868.
[50] C. Shi et al., Polymers 9 (2017) 159.
[51] O.O. Taiwo et al., Phys. Chem. Chem. Phys. 19 (2017) 22111.
[52] T.C. Bach et al., J. Energy Storage 5 (2016) 212.
[53] M. Loveridge et al., Batteries 4 (2018) 3.
[54] F. Sun et al., ACS Nano 10 (2016) 7990.
[55] J.-H. Cheng et al., J. Phys. Chem. C 121 (2017) 7761.
[56] K.-H. Chen et al., J. Mater. Chem. A 5 (2017) 11671.
[57] M. Grützke et al., ChemSusChem 8 (2015) 3433.
[58] R. Robert, P. Novák, Chem. Mater. 30 (2018) 1907.
[59] B.P. Matadi et al., J. Electrochem. Soc. 164 (2017) A2374.
[60] N. Ghanbari et al., J. Phys. Chem. C 120 (2016) 22225.
[61] L. Yang et al., ACS Appl. Mater. Interfaces 6 (2014) 12962.
[62] M. Lewerenz et al., J. Power Sources 369 (2017) 122.
[63] A. Iturrondobeitia et al., J. Phys. Chem. C 121 (2017) 21865.
[64] V.A. Agubra et al., Electrochim. Acta 149 (2014) 1.
[65] K. Jalkanen et al., Appl. Energ. 154 (2015) 160.
[66] Y. Kobayashi et al., J. Electrochem. Soc. 160 (2013) A1415.
[67] M. Zier et al., J. Power Sources 266 (2014) 198.
[68] J.-J. Woo et al., J. Electrochem. Soc. 161 (2014) A827.
[69] C. Uhlmann et al., J. Power Sources 279 (2015) 428.
[70] Q. Liu et al., RSC Adv. 6 (2016) 88683.
[71] V. Agubra, J. Fergus, Materials 6 (2013) 1310.
[72] Y. Zhang et al., ACS Energy Lett. 2 (2017) 2696.
[73] S. Jiao et al., Joule 2 (2017) 110.
[74] F. Sun et al., ACS Energy Lett. 3 (2018) 356.
[75] C.M. López et al., J. Electrochem. Soc. 159 (2012) A873.
[76] Z. Guo et al., RSC Adv. 5 (2015) 69514.
[77] C.-Y. Tang, S.J. Dillon, J. Electrochem. Soc. 163 (2016) A1660.
[78] Q. Yuan et al., Electrochim. Acta 178 (2015) 682.
[79] D. Aurbach et al., Electrochim. Acta 39 (1994) 51.
[80] D. Aurbach, A. Zaban, J. Electrochem. Soc. 141 (1994) 1808.
[81] S.S. Zhang et al., J. Power Sources 160 (2006) 1349.
[82] M.C. Smart, B.V. Ratnakumar, J. Electrochem. Soc. 158 (2011) A379.
[83] F. Xu et al., J. Electrochem. Soc. 159 (2012) A678.
[84] S.S. Zhang, J. Power Sources 161 (2006) 1385.
[85] J. Wandt et al., Mater. Today 21 (2018) 231.
[86] S.A. Kayser et al., Phys. Chem. Chem. Phys. 20 (2018) 13765.
[87] M. Gauthier et al., J. Phys. Chem. Lett. 6 (2015) 4653.
[88] A.M. Tripathi et al., Chem. Soc. Rev. 47 (2018) 736.
[89] D. Aurbach et al., J. Electrochem. Soc. 141 (1994) 603.
[90] M. Winter, Zeitschrift für Physikalische Chemie 223 (2009) 1395.
[91] D. Aurbach, J. Power Sources 89 (2000) 206.
[92] D. Anseán et al., J. Power Sources 356 (2017) 36.
[93] T. Sasaki et al., J. Electrochem. Soc. 156 (2009) A289.
[94] Y. Cui et al., ACS Appl. Mater. Interfaces 8 (2016) 5234.
[95] T. Guan et al., Appl. Energ. 177 (2016) 1.
[96] Y. Lu et al., Adv. Energy Mater. 5 (2015) 1402073.
[97] Proceedings of the workshop on lithium nonaqueous battery electrochemistry. Case Western Reserve University, CLeveland/Ohio, 1980.
[98] C.S. Rustomji et al., Science 356 (2017) 1351.
[99] L. Porz et al., Adv. Energy Mater. 7 (2017) 1701003.
[100] M. Han et al., Chem. Commun. 54 (2018) 2381.

[101] O. Tutusaus et al., ACS Energy Lett. 2 (2017) 224.
[102] W. Zhang et al., J. Am. Chem. Soc. 139 (2017) 3316.
[103] D. Wang et al., Nat. Mater. 17 (2017) 16.
[104] K.-I. Okazaki et al., ACS Energy Lett. 2 (2017) 1460.
[105] S. Rothermel et al., Energy Environ. Sci. 7 (2014) 3412.
[106] T. Placke et al., J. Electrochem. Soc. 159 (2012) A1755.
[107] X. Tong et al., Adv. Mater. 28 (2016) 9979.
[108] D.-C. Lee et al., ACS Energy Lett. 3 (2018) 794.